Han et al. *Zool. Res.* 2025, 46(6): 1304−1316
https://doi.org/10.24272/j.issn.2095-8137.2025.066
https://cstr.cn/32248.14.zr.2025.066

ZR | Zoological Research

Article Open Access

Tau impedes glioma progression by enhancing fatty acid β-oxidation-induced cellular senescence

Wan-Hong Han[1,#], Wu-Jie Zhao[1,#], Jia-Wei He[1], Wen-Peng Zhao[1], Han-Wen Lu[1], Zhen-Wei Lu[3], Xian-Sheng Qiu[3], Chen Chang[4], Ya-Ya Zhang[2], Yuan-Yuan Xie[1], Yan-Yan Geng[1], Bing-Chang Zhang[1,*], Zhan-Xiang Wang[1,*]

[1] *Department of Neurosurgery and Department of Neuroscience*, *Fujian Key Laboratory of Brain Tumors Diagnosis and Precision Treatment*, *Xiamen Key Laboratory of Brain Center*, *the First Affiliated Hospital of Xiamen University*, *School of Medicine*, *Xiamen University*, *Xiamen*, *Fujian* 361102, *China*

[2] *Department of Medical Oncology*, *the First Affiliated Hospital of Xiamen University*, *Xiamen*, *Fujian* 361102, *China*

[3] *Department of Neurosurgery and Department of Neuroscience*, *Fujian Key Laboratory of Brain Tumors Diagnosis and Precision Treatment*, *Xiamen Key Laboratory of Brain Center*, *the First Affiliated Hospital of Xiamen University*, *Fujian Medicine University*, *Fuzhou*, *Fujian* 350122, *China*

[4] *Department of Pathology*, *Shaanxi Provincial People's Hospital*, *Xi'an*, *Shaanxi* 710068, *China*

ABSTRACT

Tau (*MAPT*) expression is inversely associated with glioma malignancy and patient survival. However, the molecular mechanisms underlying this correlation are yet to be fully investigated. This study demonstrated that tau suppressed glioma cell proliferation both *in vitro* and *in vivo*. Mechanistically, tau promoted fatty acid β-oxidation, leading to DNA damage and glioma cellular senescence. Functional analyses revealed that tau interacted with carnitine palmitoyltransferase 1A (CPT1A), enhancing CPT1 enzymatic activity and thereby accelerating lipid catabolism. These findings establish tau as a regulator of metabolic reprogramming and senescence in glioma via CPT1-dependent β-oxidation and support its potential as a therapeutic target in glioma management

Keywords: Glioma; Tau; CPT1A; Cellular senescence; Fatty acid β-oxidation

INTRODUCTION

Gliomas are primary brain tumors presumed to originate from neuroglial cells and are characterized by diffuse infiltration of surrounding brain tissue. According to the World Health Organization (WHO) classification, gliomas are stratified from low-grade (grade II) to high-grade (grade IV) lesions, with glioblastoma (GBM) representing the most aggressive subtype (Ceccarelli et al., 2016). GBM exhibits rapid progression and poor prognosis, with a median overall survival of approximately 15 months (Khosla, 2016). Current standard-of-care therapies include surgical resection, radiotherapy, and alkylating chemotherapy (Weller et al., 2015), which offer limited long-term efficacy. Consequently, a deeper understanding of glioma pathogenesis and the identification of novel therapeutic targets remain urgent priorities.

Lipid droplets (LDs) serve as intracellular reservoirs for neutral lipids and are essential for sustaining cellular viability under nutrient deprivation and metabolic stress (Velázquez et al., 2016). Accumulation of LDs correlates with glioma malignancy and is associated with unfavorable clinical outcomes (Geng et al., 2016). Genetic inhibition of LD-associated regulators, such as SOAT1, DGAT1, and FABP7, has been shown to impair glioma progression, underscoring the critical role of LDs in supporting tumor cell survival within the central nervous system microenvironment (Cheng et al., 2020; Miska & Chandel, 2023; Shakya et al., 2021).

Carnitine palmitoyltransferase 1A (CPT1A), a key member of the long-chain acyltransferase family, catalyzes the transfer of long-chain acyl groups from acyl-CoA to carnitine, enabling their translocation across the mitochondrial membrane via the carnitine transporter. This reaction constitutes the rate-limiting step for mitochondrial import and subsequent β-oxidation of long-chain fatty acids (Casals et al., 2016). Fatty acid β-oxidation (FAO) is a primary mitochondrial pathway for catabolizing long-chain fatty acids, supplying reducing equivalents to fuel the tricarboxylic acid (TCA) cycle and oxidative phosphorylation and stimulating hepatic synthesis of

Received: 19 May 2025; Accepted: 27 October 2025; Online: 28 October 2025

Foundation items: This work was supported by the National Natural Science Foundation of China (82072777), Fujian Provincial Clinical Research Center for Brain Diseases (2021FJSLCYX01), Xiamen Clinical Research Center for Neurological Diseases (2021XMSLCYX01) Project of Xiamen Cell Therapy Research (3502Z20214001), and Raman Medical Collaboration Project of the First Affiliated Hospital of Xiamen University (XFLM2023005)

[#]Authors contributed equally to this work

*Corresponding authors, E-mail: bczhang@xmu.edu.cn; wangzx@xmu.edu.cn

ketone bodies to provide ATP (Houten et al., 2016). Beyond its canonical role in energy metabolism, FAO has recently been linked to the regulation of cellular senescence, partly through the induction of P16 expression (Yamauchi et al., 2024).

The microtubule-associated protein tau, encoded by the *MAPT* gene, has been extensively studied in the context of neurodegenerative disease (Bunker et al., 2004). However, growing evidence also implicates tau in tumor biology, particularly in gliomas (Hedna et al., 2022). Elevated tau expression is strongly associated with favorable prognostic markers and prolonged survival on glioma patients (Gargini et al., 2019). Tau levels correlate with isocitrate dehydrogenase (IDH) mutations in infiltrating gliomas and are linked to reduced migratory capacity of tumor cells (Nakata et al., 2020), suggesting a potential tumor-suppressive role in the glioma microenvironment. Recent studies have uncovered previously unappreciated roles for tau in lipid homeostasis modulation, particularly in the context of neurodegenerative pathologies and glial function in *Drosophila* models. Overexpression of human tau in glial cells disrupts LD architecture and glial morphology in response to neuron-driven reactive oxygen species (ROS) (Goodman et al., 2024). Consistently, Li et al. (2024) reported an accumulation of unsaturated lipids within LDs in tauopathy mouse brains and cultured neurons. However, the role of tau in lipid metabolic regulation within gliomas remains largely unexplored.

This study identified tau as a regulator of lipid metabolism in glioma cells, where it stimulates FAO, triggering DNA damage and cellular senescence. Mechanistic analysis reveals that tau physically interacts with CPT1A, promoting its enzymatic activity and thereby accelerating mitochondrial fatty acid catabolism. These findings define a previously unrecognized tau-CPT1A axis that links lipid metabolic reprogramming to glioma cell fate and suggest tau as a potential metabolic target and biomarker in glioma pathophysiology.

MATERIALS AND METHODS

Cell culture

Human glioma cell lines U87 and T98G were purchased from the American Type Culture Collection (ATCC) and maintained in Dulbecco's Modified Eagle Medium (DMEM, Cytiva, USA) supplemented with 10% fetal bovine serum (FBS, ABW, China) and 1% penicillin-streptomycin (Gibco, USA) at 37°C in a humidified 5% CO_2-containing atmosphere. Patient-derived primary GBM38 cells were isolated and cultured according to the protocol described by Xiang et al. (2022). Tumor tissues were collected with informed consent from patients and with approval from the Ethics Committee of the First Affiliated Hospital of Xiamen University (China).

Lentiviral packaging and cell infection

Full-length human tau and control constructs were cloned into the pLVX-IRES-Puro-Flag lentiviral vector. Single-guide RNAs (sgRNAs) targeting human *MAPT* and *CPT1A* were inserted into the GV708 vector. (sgRNA sequences are listed in Supplementary Table S1). Lentiviral packaging was performed in HEK293T cells, with the packaged virus then used to infect U87, GBM38, or T98G cells, as described in previous research (Han et al., 2025).

Probes and dyes

MitoTracker Green (Beyotime, China) was used to label mitochondria at a final concentration of 100 nmol/L in FluoroBrite™ DMEM (Gibco, USA). MitoSOX Red (Beyotime, China) was applied at 5 μmol/L in FluoroBrite™ DMEM to detect mitochondrial ROS. FAO Blue (Funakoshi, Japan) was used to assess FAO activity at 10 μmol/L in Hank's Balanced Salt Solution (Gibco, USA). LD staining was performed using BODIPY 493/503 (Beyotime, China).

Human glioma tissue microarray (TMA) and immunohistochemistry

Glioma tissue samples were collected from patients treated at the First Affiliated Hospital of Xiamen University. Written informed consent was obtained from all patients or their legal guardians. All procedures conformed to the Declaration of Helsinki and were approved by the Ethics Committee of the First Affiliated Hospital of Xiamen University. Immunohistochemical staining of tau on the TMA was conducted by Servicebio Technology (China).

Cell viability assay (CCK-8)

Cells were seeded in 96-well plates (5 000 cells/well) and cultured for 72 h. Following this, the cells were incubated with medium containing 10% Cell Counting Kit-8 reagent (CCK-8, ApexBio, USA) for 1 h at 37°C. Absorbance was measured at 450 nm using an iMark™ Microplate Reader (Bio-Rad, USA).

Colony formation assay

Cells were seeded into plates at a density of 800 cells per well and cultured for 14 days. Colonies were fixed with methanol for 15 min and subsequently stained with 0.5% crystal violet for 20 min before imaging and quantification.

RNA sequencing (RNA-seq) and gene enrichment analysis

U87 glioma cells overexpressing human tau or an empty vector (3×10^6 cells per sample) were subjected to transcriptomic profiling. Three biological replicates were prepared per condition. Total RNA was extracted using TRIzol reagent (Invitrogen, USA), and RNA quantity and purity were assessed using a NanoDrop ND-1000 spectrophotometer (NanoDrop, USA). RNA integrity was evaluated using the Bioanalyzer 2100 system (Agilent, USA), with all samples exhibiting RNA integrity numbers (RIN) greater than 7.0 and confirmed by denaturing agarose gel electrophoresis. Poly(A) RNA was purified from 1 μg of total RNA using Dynabeads Oligo (dT)25-61005 (Thermo Fisher, USA) through two rounds of purification. The purified RNA was fragmented at 94°C for 5–7 min using the Magnesium RNA Fragmentation Module (New England Biolabs (NEB), USA). The cleaved RNA fragments were reverse-transcribed to create the cDNA using SuperScript™ II Reverse Transcriptase (Invitrogen, USA), followed by second-strand synthesis using *E. coli* DNA polymerase I (NEB, USA), RNase H (NEB, USA), and dUTP Solution (Thermo Fisher, USA) to generate uracil-containing double-stranded DNA. A single adenine base was added to the blunt ends of each strand to facilitate adaptor ligation. Indexed adapters containing a thymine overhang were ligated to the A-tailed fragments. Following adapter ligation, size selection was performed using AMPure XP beads(Beckman Coulter, USA). U-labeled second strands were selectively degraded using heat-labile UDG enzyme (NEB, USA), and the resulting products were polymerase chain reaction (PCR)-amplified under the following conditions: initial denaturation at 95°C for 3 min; eight cycles of denaturation at 98°C for 15 s, annealing at 60°C for 15 s, and extension at 72°C for 30 s,

followed by a final extension at 72°C for 5 min. The average insert size for the final cDNA library was 300±50 bp. Paired-end sequencing (2×150 bp, PE150) was performed on the Illumina NovaSeq™ 6000 platform (LC-Bio Technology, China) following the vendor's recommended protocols.

Raw sequencing reads were filtered using fastp (https://github.com/OpenGene/fastp) to eliminate reads containing adaptor contamination, low-quality bases, or undetermined bases, using default parameters. Clean reads were aligned to the human reference genome (GRCh38) using HISAT2 (https://ccb.jhu.edu/software/hisat2), and transcript assembly was performed using StringTie (https://ccb.jhu.edu/software/stringtie) with default parameters. All transcriptomes were merged using gffcompare (https://github.com/gpertea/gffcompare/) to generate a unified reference annotation. Expression levels of transcripts were quantified by StringTie and expressed as fragments per kilobase of transcript per million mapped reads (FPKM) (FPKM=[total exon fragments/mapped reads (millions)×exon length (kB)]). Differential gene expression analysis was conducted using DESeq2 for group comparisons and edgeR for pairwise comparisons. Genes with a false discovery rate (FDR)<0.05 and absolute fold change≥2 were considered significantly differentially expressed genes (DEGs). Functional enrichment of DEGs was performed using the Kyoto Encyclopedia of Genes and Genomes (KEGG) database (http://www.kegg.jp/kegg).

Western blot analysis

Western blotting was performed as described previously (Han et al., 2025). Primary antibodies used included: CPT1A (Proteintech, China, 1:1 000), Tau (Abcam, USA, 1:1 000), LamininB1 (Proteintech, China, 1:1 000), P21 (Proteintech, China, 1:1 000), and β-actin (Sigma, USA, 1:20 000). Secondary antibodies used included: anti-mouse (Invitrogen, USA, 1:10 000) and anti-rabbit (Invitrogen, USA, 1:10 000).

Immunofluorescence staining

Cells or slices were fixed in 4% paraformaldehyde (PFA) for 15 min, then incubated with blocking buffer (0.3% Triton-X-100, and 2% BSA in PBS) for 1.5 h at room temperature. Cells or slices were further incubated with antibodies against γ-H2AX (CST, USA, 1:500) and Ki-67 (CST, USA, 1:250), followed by incubation with appropriate fluorescence-labeled secondary antibodies (Yeasen, China, 1:200). Subsequently, samples were incubated with antifade mounting medium with Hoechst 33342 (Beyotime, China) for 10 min, followed by image acquisition using a microscope (Invitrogen, USA).

Immunoprecipitation

Protein lysates were incubated overnight at 4°C with the indicated antibodies or control IgG (Proteintech, China). Protein A/G magnetic beads (Thermo Scientific, USA) were then added and incubated for 1 h at 4°C. Beads were washed with NP-40 buffer, and immunoprecipitated proteins were subjected to western blotting or liquid chromatography-mass spectrometry (LC-MS). For western blotting, beads were washed again with NP-40 buffer and resuspended in SDS loading buffer prior to electrophoresis.

LC-MS analysis of tau-interacting proteins

Cell lysates were immunoprecipitated with anti-Tau antibody or control IgG. Immunoprecipitates were resolved by sodium dodecyl sulfate-polyacrylamide gel electrophoresis (SDS-PAGE), and protein bands were visualized by Coomassie blue staining after electrophoresis into the gel (~1 cm). Stained gel slices were thoroughly washed and subjected to in-gel trypsin digestion. The samples were analyzed using the nanoElute system (Bruker , USA) coupled with a timsTOF Pro mass spectrometer (Bruker,USA) equipped with a CaptiveSpray ion source. Digested peptides were dissolved in 10 μL of 0.1% formic acid and auto-sampled onto a homemade C18 column (35 cm×75 μm i.d., 1.9 μm, 100Å). The samples were then eluted using a linear 60 min gradient of 3%–35% acetonitrile in 0.1% formic acid at a flow rate of 300 nL/min. Mass spectra were acquired in PASEF mode, and raw data were analyzed using Peaks Studio X (Bioinformatics Solutions Inc, Canada) against the UniProt human protein database (https://www.uniprot.org/).

Lipidomic analysis

Lipids were extracted from approximately 1×10^6 U87 cells transduced with either a tau-overexpressing vector or control vector, following a modified Bligh and Dyer protocol as described previously (Miao et al., 2023). Briefly, cells were homogenized in 750 μL of chloroform:methanol: Milli-Q H_2O (3:6:1) (v/v/v) and incubated at 1 500 r/min for 1 h at 4°C. After incubation, 350 μL of deionized water and 250 μL of chloroform were added to induce phase separation. Samples were centrifuged, and the lower organic phase containing lipids was collected into a clean tube. Lipid extraction was repeated by adding 450 μL of chloroform to the residual aqueous phase, and the lipid extracts were pooled and dried in a SpeedVac (Thermofisher Scientific, USA) under OH mode. Samples were stored at −80°C until analysis. The upper aqueous phase and remaining cell pellet were dried in a SpeedVac(Thermofisher Scientific, USA)under H_2O mode. Total protein content was determined from the dried pellet using the Pierce® BCA Protein Assay Kit (Thermofisher Scientific, USA) according to the manufacturer's protocols.

Lipidomic profiling was performed by LipidALL Technologies (China) using Jasper high-performance liquid chromatography (HPLC)(Sciex, USA) coupled with a Sciex TRIPLE QUAD 4500 MD mass spectrometer (Sciex, USA), as described previously (Lam et al., 2021). Lipid classes were separated by normal phase (NP)-HPLC using a TUP-HB silica column (i.d. 150 mm×2.1 mm, 3 μm) with the following conditions: mobile phase A (chloroform: methanol: ammonium hydroxide, 89.5:10:0.5) and mobile phase B (chloroform: methanol: ammonium hydroxide: water, 55:39:0.5:5.5). Multiple reaction monitoring (MRM) transitions were established for comparative analysis of various lipids. Individual lipid species were quantified by referencing to spiked internal standards. d9-PC32:0(16:0/16:0), PE 34:0, dic8-PI, d31-PS, C17:0-PA, DMPG, CL-14:0, C14-BMP, C12-SL, C17-LPC, C17-LPE, C17:1-LPI, C17:0-LPA, C17:1-LPS, C17-Cer, C12-SM, d17:1-S1P, d17:1-Sph, C8-GluCer, C8-LacCer, Gb3-d18:1/17:0, d3-16:0 carnitine, and DAG(18:1/18:1)-d5 were obtained from Avanti Polar Lipids. GM3-d18:1/18:0-d3 was purchased from Matreya LLC. Free fatty acids (FFAs) were quantitated using d31-16:0 (Sigma-Aldrich, USA), while d6-CE 18:0 and TAG (16:0)3-d5 were obtained from CDN isotopes, Canada.

Drug affinity responsive target stability (DARTS) assay

U87 cells overexpressing tau or control vector were harvested in ice-cold M-PER lysis buffer (Thermo Scientific, USA) supplemented with a protease inhibitor cocktail (Roche, Switzerland). Following 10 min lysis, lysates were centrifuged at 18 000 ×*g* and 4°C for 10 min to remove debris and DNA.

Supernatants were collected and incubated with either 10 mmol/L carnitine chloride (Sigma, USA) or ddH_2O at room temperature for 30 min. Subsequently, samples were digested with pronase (1 μg/500 μg protein) for 10 min at room temperature, followed by the addition of 5×SDS loading buffer to stop the reaction. Protected proteins were analyzed by western blotting using CPT1A antibody, with β-actin acting as a loading control.

CPT1 activity assessment

U87 cells (5×10^6 per sample) overexpressing tau or control vector and subcutaneous xenograft tumor tissues (0.1 g per sample) were used for CPT1 activity measurement using a CPT1 Activity Kit (Zikerbio, China) according to the manufacturer's instructions.

Senescence β-galactosidase (staining

Senescence β-galactosidase staining was performed using a Senescence β-Galactosidase Staining Kit (Beyotime, China) according to the manufacturer's instructions.

Subcutaneous xenograft model

U87 cells stably overexpressing tau or control vector (5×10^6) were resuspended in 100 μL of PBS and subcutaneously injected into 6-week-old female BALB/c-nude mice. After 3 weeks, tumors were harvested and subjected to western blot analysis, β-galactosidase staining, CPT1A activity assay, BODIPY staining, and quantification of triacylglycerol (TAG) and FFAs. Each experimental group comprised seven mice; during statistical analysis, the maximum and minimum tumor volumes were excluded, leaving five samples per group for downstream analysis and molecular experiments. Female nude mice were obtained from Xiamen University Animal Experiment Center and housed under a 12 h light/dark cycle at 20°C and 40% humidity. All animal experiments were reviewed and approved by the Animal Ethics Committee of Xiamen University (XMULAC20250002).

Intracranial xenograft model

U87 cells expressing luciferase and either tau or control vector were stereotactically implanted (2×10^5 cells per mouse) into the brains of 6-week-old female BALB/c-nude mice. On day 14 post-implantation, mice were injected intraperitoneally with a luciferin solution (150 mg/kg), and bioluminescence imaging was conducted using the AniView 100 Pro multimodal *in vivo* imaging system (Biolight Biotechnology, China). Images were analyzed using AniView Pro software (Biolight Biotechnology, China).

Protein-protein docking analysis

Molecular docking between human tau and CPT1A was performed using the ZDOCK v.3.0.2 web server (https://zdock.wenglab.org/). Predicted three-dimensional (3D) structures were sourced from the AlphaFold Protein Structure Database (https://alphafold.ebi.ac.uk/). Tau was truncated into four functional domains using PyMOLv.3.1.4.1 (https://www.pymol.org/): N-terminal region (residues 1–103), proline-rich region (residues 103–244), microtubule-binding region (residues 244–368), and C-terminal region (residues 369–441). Each domain was saved separately in PDB format and uploaded to the ZDOCK server, with "Skip residue selection" enabled and default parameters applied. After calculations were completed, the scoring results and top-ranked predicted docking poses were downloaded. Subsequently, the predicted complexes were visualized using PyMOLv.3.1.4.1 (https://www.pymol.org/): and potential interaction sites were highlighted to assess the binding interfaces between tau domains and CPT1A.

Datasets and data analysis

RNA expression data and overall survival rates were obtained from public cancer/glioma datasets, including the Chinese Glioma Genome Atlas (CGGA, http://www.cgga.org.cn/) and the Cancer Genome Atlas (TCGA) via the UCSC Xena platform (https://xena.ucsc.edu/).

Statistical analysis

All experimental data were statistically analyzed using GraphPad Prism v.8.0. Standard deviation (SD) was utilized to assess data variability in heatmaps, while standard error of the mean (SEM) was employed to evaluate sample mean precision. Quantitative data are presented as mean±SEM. Unpaired *t*-tests were conducted for non-paired parametric comparisons between two groups. Mann-Whitney *U* tests were applied for non-paired non-parametric comparisons between two groups. One-way and two-way analysis of variance (ANOVA), followed by *post hoc* tests, were utilized for comparisons involving multiple groups. Kaplan-Meier survival analysis was executed using log-rank analysis. Statistical significance was determined as follows: ****: $P<0.0001$; ***: $P<0.001$; **: $P<0.01$; *: $P<0.05$; ns: Not significant.

RESULTS

Tau expression is down-regulated in glioma patients

To delineate the clinical relevance of tau in glioma, transcriptomic datasets from the UCSC Xena platform were examined. *MAPT* mRNA expression was significantly reduced in GBM relative to normal brain tissue (Supplementary Figure S1A). Analysis across the TCGA and CGGA cohorts further revealed a stepwise decline in *MAPT* mRNA levels with increasing WHO tumor grade (Figure 1A; Supplementary Figure S1B). Furthermore, stratification by histological subtype, IDH mutation status, 1p/19q status, and MGMT status also demonstrated significant differences in MAPT levels (Figure 1B–E; Supplementary Figure S1C–F). Notably, *MAPT* expression showed a strong positive association with glioma patient survival, with lower *MAPT* levels corresponding to reduced overall survival (Figure 1F; Supplementary Figure S1G). Furthermore, univariate Cox proportional hazards analysis identified *MAPT* as a significant prognostic indicator of glioma outcome (Supplementary Tables S1, S2).To validate these transcriptomic observations, immunohistochemical analysis was performed on a glioma TMA cohort. Results indicated that tau protein abundance was significantly diminished in glioma compared to normal brain and progressively declined with advancing tumor grade (Figure 1G, H). Immunoblotting of glioma cell lines and primary GBM38 cells similarly revealed markedly lower tau protein levels relative to normal human astrocytes (NHAs) (Figure 1I, J). Collectively, these data demonstrate that tau is transcriptionally and translationally down-regulated in glioma and inversely correlates with malignancy.

Tau suppresses glioma cell proliferation and tumor growth

Given the observed reduction of tau in glioma, functional studies were performed to assess its biological impact. Tau

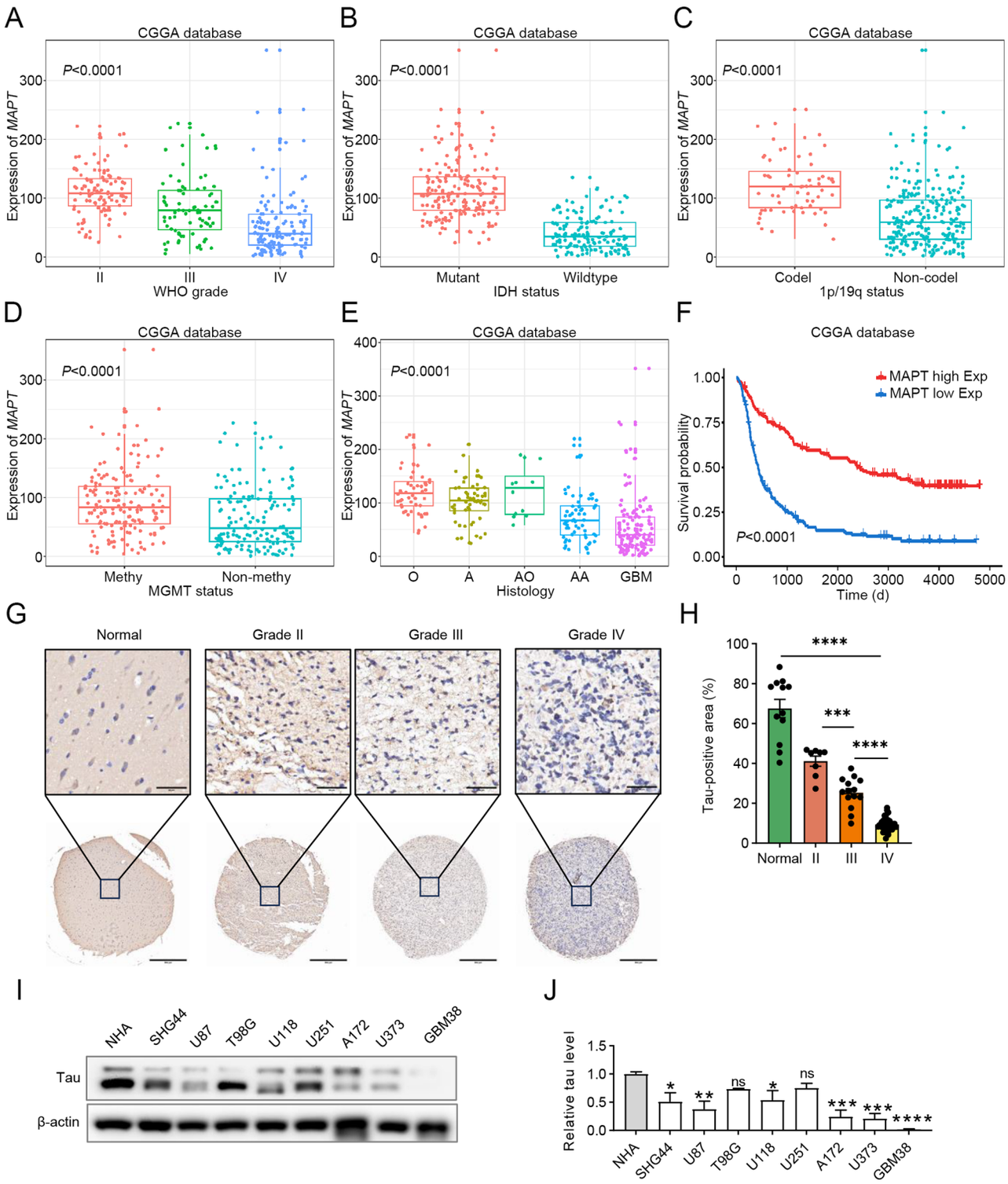

Figure 1 Tau is down-regulated in glioma

A: *MAPT* expression across WHO grades II (*n*=103), III (*n*=79), and IV (*n*=139) gliomas in the CGGA database. Data were analyzed by one-way ANOVA. B: *MAPT* expression across histological subtypes: oligodendroglioma (O, *n*=52), astrocytoma (A, *n*=56), anaplastic oligodendroglioma (AO, *n*=12), anaplastic astrocytoma (AA, *n*=62), and glioblastoma (GBM, *n*=139). Data were analyzed by one-way ANOVA. C: *MAPT* expression stratified by IDH mutation status: mutant (*n*=175) and wild-type (*n*=149). Data were analyzed by unpaired *t*-test. D: *MAPT* expression stratified by 1p/19q status: codel (*n*=67) and non-codel (*n*=250). Data were analyzed by unpaired *t*-test. E: *MAPT* expression stratified by MGMT promoter methylation status: methylated (methy, *n*=157) and unmethylated (non-methy, *n*=149). Data were analyzed by unpaired *t*-test. F: Kaplan-Meier analysis of overall survival in patients with high (*n*=156) versus low (*n*=157) *MAPT* expression (CGGA). G: Representative tau immunohistochemical images from tissue microarrays (TMA). Scale bar: 50 μm or 500 μm. H: Quantification of tau-positive area (%) from panel G across normal brain (*n*=12), grade II (*n*=8), grade III (*n*=14), and grade IV (*n*=38) glioma tissues. I, J: Western blot analysis (I) and densitometric quantitation (J) of tau protein levels in NHA and glioma cell lines (*n*=3 per group). β-actin was used as an internal loading control. *n*=3 per group. Data are presented as mean±SEM. *: *P*<0.05; **: *P*<0.01; ***: *P*<0.001; ****: *P*<0.0001; ns: Not significant.

expression was ectopically up-regulated in U87 and GBM38 cells which exhibit relatively low endogenous levels, and silenced in T98G cells, which exhibit relatively higher basal levels (Figure 2A). Cell proliferation assays revealed that overexpression of tau significantly inhibited U87 and GBM38 cell proliferation (Figure 2B), whereas knockdown of tau promoted T98G cell proliferation (Figure 2B). These findings were further supported by Ki-67 immunostaining (Figure 2C–F) and colony formation assays (Figure 2G). Additionally, tau overexpression suppressed tumor progression in both intracranial (Figure 2H–J) and subcutaneous xenograft models (Figure 2K–M). Consistent with the *in vitro* observations, tumor sections from subcutaneous models further exhibited diminished Ki-67 positivity in tau-overexpressing cells (Figure 2N–O).These findings collectively indicate that tau functions as a negative regulator of glioma cell proliferation and tumor growth.

Tau overexpression induces DNA damage and cellular senescence in glioma cells

To elucidate the molecular mechanisms underlying tau-mediated suppression of glioma cell proliferation, transcriptomic profiling was conducted in U87 cells overexpressing tau or control vector. Tau overexpression resulted in the up-regulation of 1 698 genes and down-regulation of 1 658 genes. Gene Ontology (GO) enrichment analysis identified significant enrichment in DNA damage response, DNA repair, and double-strand break repair pathways in tau-overexpressing cells (Figure 3A), suggesting the induction of genotoxic stress. KEGG pathway analysis further revealed enrichment of DEGs in pathways associated with cell cycle regulation, focal adhesion, cellular senescence, actin cytoskeleton remodeling, and endocytosis (Figure 3B). Given that DNA damage is a potent driver of cellular senescence, these data implicate tau in promoting DNA damage-induced cellular senescence.

To experimentally validate this hypothesis, γH2AX immunofluorescence staining was conducted. A marked increase in γH2AX-positive cells was observed in tau-overexpressing U87 and GBM38 cells, whereas tau knockdown in T98G cells led to a decrease in γH2AX signal (Figure 3C–F). In parallel, expression of p21, a negative regulator of the cell cycle, was up-regulated following tau overexpression and down-regulated following tau silencing (Figure 3G). Senescence-associated β-galactosidase staining further demonstrated that the proportion of senescent cells in U87, GBM38, and T98G cultures was modulated in accordance with tau expression levels (Figure 3H–K). These observations were corroborated in vivo, where tau-overexpressing subcutaneous xenograft tumors exhibited elevated γH2AX, increased p21 expression, and higher β-galactosidase positivity (Figure 3L–O). Together, these findings indicate that tau induces DNA damage and promotes cellular senescence in glioma.

Tau enhances FAO in glioma cells

Having established that tau overexpression induces DNA damage and cellular senescence in glioma, further investigation was undertaken to elucidate the metabolic mechanisms involved. Proteomic and lipidomic datasets from a study of treatment-naïve GBM specimens (Wang et al., 2021) were reanalyzed. Based on tau protein levels, samples were stratified into tau-high (55 cases), tau-low (44 cases), and paracancerous control tissues (10 cases) (Supplementary Figure S2A). Subsequent lipidomic profiling revealed that increasing tau levels were associated with a significant decrease in tissue glycerides and a concomitant elevation in the levels of glycerophospholipids and sphingomyelin (Supplementary Figure S2B), suggesting a potential link between tau expression and lipid metabolic remodeling.

To verify whether tau modulates lipid metabolism in glioma, lipidomic analyses were performed on U87 cells transduced with either tau or control vector. Results demonstrated that tau overexpression led to a pronounced alteration in lipid composition (Figure 4A), including a significant decrease in TAG and FFAs, along with a marked accumulation of acylcarnitine. Given that TAG serves as a storage form of FFAs stored in LDs, and acylcarnitine represents the activated form of FFAs committed to mitochondrial oxidation, these findings suggest that tau enhances fatty acid catabolism. Indeed, consistent with this hypothesis, tau overexpression led to a significant reduction in LD number, whereas tau knockdown increased LD abundance (Figure 4B–E). *In vivo*, subcutaneous tumors derived from tau-overexpressing glioma cells also displayed decreased LD content, along with reduced TAG and FFA levels (Supplementary Figure S3A–D). FAO Blue staining, a fluorescent indicator of FAO, revealed increased signal intensity in tau-overexpressing U87 and GBM38 cells (Figure 4F–H) and reduced signal following tau depletion in T98G cells (Figure 4I, J), further supporting enhanced FAO activity. In parallel, mitochondrial ROS levels, assessed by MitoSOX Red fluorescence (Beyotime, China), were significantly elevated in tau-overexpressing U87 and GBM38 cells (Figure 4K–M) and decreased upon tau down-regulation in T98G cells (Figure 4K, N). Collectively, these findings suggest that tau stimulates mitochondrial FAO in glioma cells, leading to enhanced lipid catabolism and reduced LD accumulation.

Tau binds to CPT1A and enhances its enzymatic activity

To elucidate the molecular basis by which tau promotes FAO and induces cellular senescence in glioma, protein interaction screening was conducted to identify functional mediators of this metabolic shift. Given the structural characteristics of tau and its capacity to engage in protein-protein interactions, it was hypothesized that tau may modulate FAO through direct binding to lipid-metabolic enzymes. Immunoprecipitation combined with LC-MS in U87 cells identified eight tau-associated proteins involved in fatty acid metabolism. Among these, CPT1A, which catalyzes the conversion of FFAs to acyl-CoA, emerged as a prominent candidate (Figure 5A). Further verification confirmed the interaction between tau and CPT1A (Figure 5B, C). Notably, CPT1A and tau exhibited substantial intracellular co-localization (Figure 5D). DARTS analysis further demonstrated that tau binds to CPT1A in both the presence and absence of carnitine (Figure 5E), indicating substrate-independent complex formation. To define the structural basis of this interaction, molecular docking simulations were performed using truncated tau constructs (Figure 5F). The microtubule-binding region exhibited the highest predicted binding affinity for CPT1A, suggesting a role in mediating the interaction. Furthermore, overexpression of tau significantly increased CPT1 enzymatic activity in both *in vivo* and *in vitro* models without altering CPT1A expression (Figure 5G–I).

Tau induces DNA damage and cellular senescence in a CPT1A-dependent manner

To determine whether tau-induced DNA damage and cellular

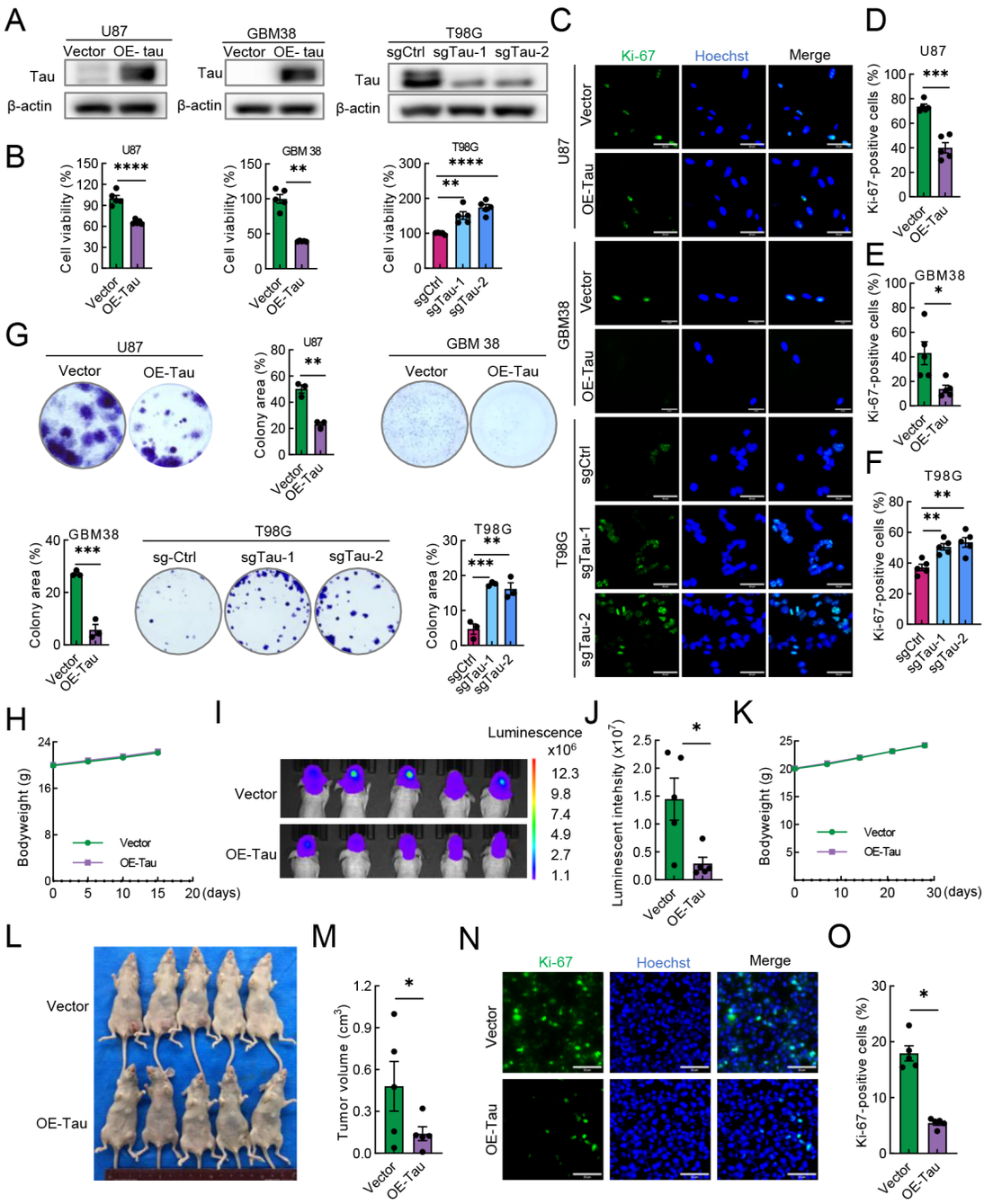

Figure 2 Tau suppresses glioma cell proliferation and tumor growth

A: Western blot analysis of tau expression in U87, GBM38, and T98G cells following lentiviral infection. B: Cell viability of U87, GBM38, and T98G cells following infection. *n*=5 per group. C–F: Representative images (C) and quantification (D–F) of Ki-67 immunofluorescence staining in U87, GBM38, and T98G cells. Scale bar: 50 μm. *n*=5 per group. G: Representative images and quantification of colony formation in infected U87, GBM38, and T98G cells assessed by crystal violet staining. *n*=3 per group. H: Body weight of nude mice after intracranial injection of U87 cells infected with control or tau-expressing vectors. *n*=5 per group. I, J: Representative bioluminescence images (I) and quantification (J) of intracranial tumor growth at day 14 post-implantation. *n*=5 per group. K: Body weight of nude mice following subcutaneous implantation of U87 cells infected with control or tau-expressing vectors. *n*=5 per group. L, M: Representative tumor images (L) and volume quantification (M) from subcutaneous xenografts at day 28 post-implantation. *n*=5 per group. N, O: Representative images (N) and quantification (O) of Ki-67 staining in subcutaneous tumors. Scale bar: 50 μm. *n*=5 per group. Data are presented as mean±SEM, analyzed by unpaired *t*-test (for U87 and GBM38 in B, G, D, E, J, M, and O) and one-way ANOVA (for T98G in B, G, and F). *: $P<0.05$; **: $P<0.01$; ***: $P<0.001$; ****: $P<0.0001$.

senescence depend on CPT1A, U87 cells were engineered to overexpress tau in the context of CPT1A down-regulation (Figure 6A). Results demonstrated that down-regulation of CPT1A effectively blocked the ability of tau to reduce LD number (Figure 6B, C), induce DNA damage (Figure 6D, E), suppress proliferation (Figure 6F–H), and promote senescence (Figure 6I, J). Moreover, inhibition of CPT1 activity using etomoxir sodium salt similarly abrogated the effects of tau overexpression (Supplementary Figure S4A–C). These findings establish that tau-induced cellular senescence and growth inhibition are dependent on functional CPT1A.

In summary, this study demonstrated that tau directly binds

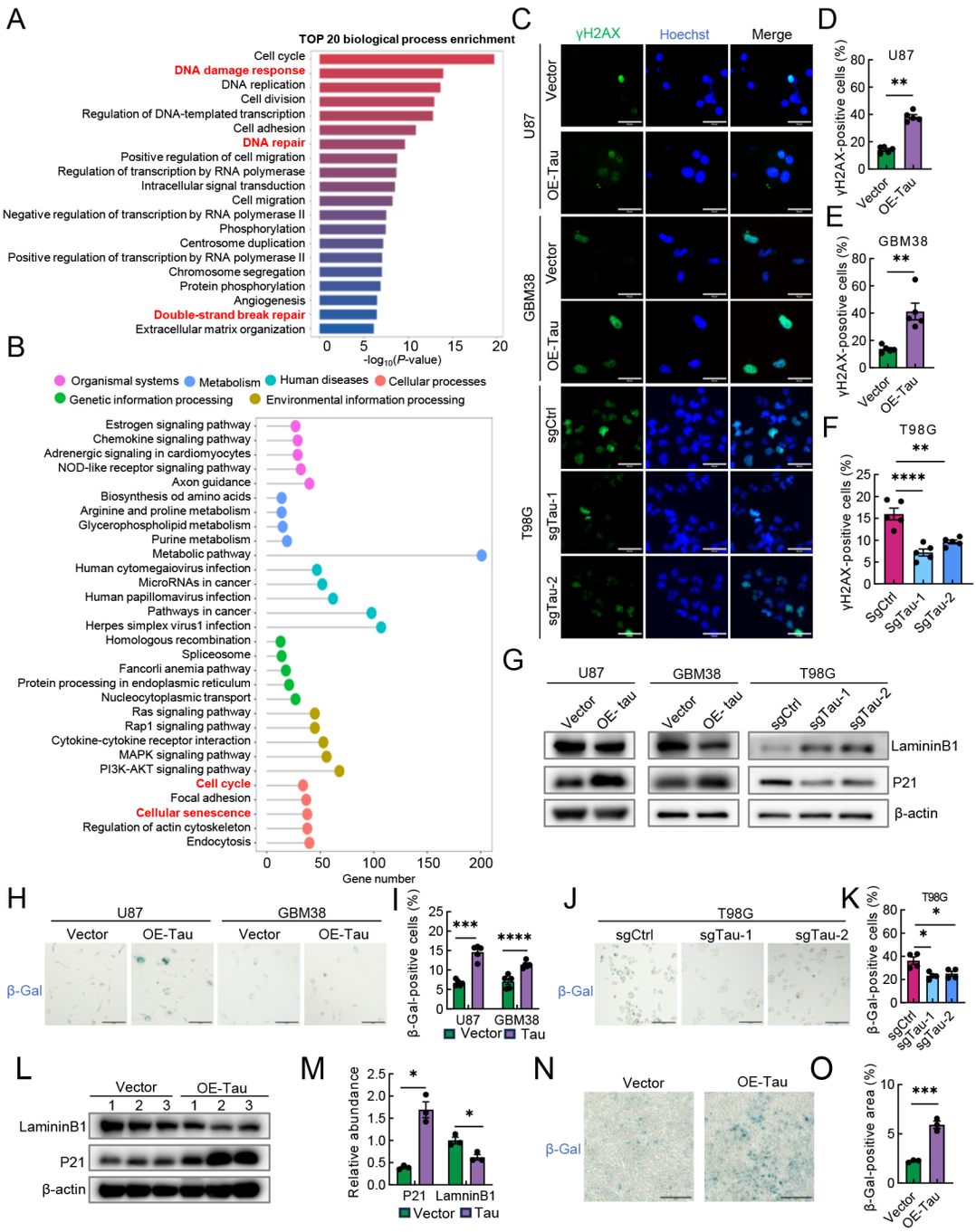

Figure 3 Tau overexpression induces DNA damage and glioma cellular senescence

A: Top 20 GO biological processes enriched among differentially expressed genes (DEGs) following tau overexpression. B: KEGG pathway enrichment analysis of tau-induced DEGs. C–F: Representative γH2AX immunofluorescence images (C) and quantification of γH2AX-positive nuclei (D–F) in U87, GBM38, and T98G cells transfected as indicated. Scale bar: 50 μm. *n*=5 per group. G: Representative western blots of senescence markers in U87, GBM38, and T98G cells transfected as indicated. H, I: Representative β-galactosidase staining (H) and quantification of β-galactosidase-positive cells (I) in U87 and GBM38 cells infected with control or tau-expressing plasmid. Scale bar: 200 μm. *n*=5 per group. J, K: Representative β-galactosidase staining (J) and quantification of β-galactosidase-positive cells (K) in T98G cells infected with sgctrl or sgTau plasmid. Scale bar: 200 μm. *n*=5 per group. L, M: Representative western blots (L) and quantification (M) of senescent markers in subcutaneous tumor xenografts. *n*=3 per group. N, O: Representative β-galactosidase staining images (N) and quantification (O) of β-galactosidase-positive cells in subcutaneous tumor xenografts. Scale bar: 200 μm. *n*=3 per group. Data are presented as mean±SEM, analyzed by unpaired *t*-test (for D, E, I, M, and O) and one-way ANOVA (for F and K). *: $P<0.05$; **: $P<0.01$; ***: $P<0.001$; ****: $P<0.0001$.

CPT1A and enhances its enzymatic activity, thereby accelerating fatty acid β-oxidation. This metabolic reprogramming leads to elevated DNA damage and senescence, ultimately suppressing glioma progression *in vivo* (Figure 6K).

DISCUSSION

Emerging evidence demonstrates an inverse relationship between tau expression, glioma progression, and patient survival (Zaman et al., 2019). However, the molecular mechanisms by which tau influences glioma biology remain

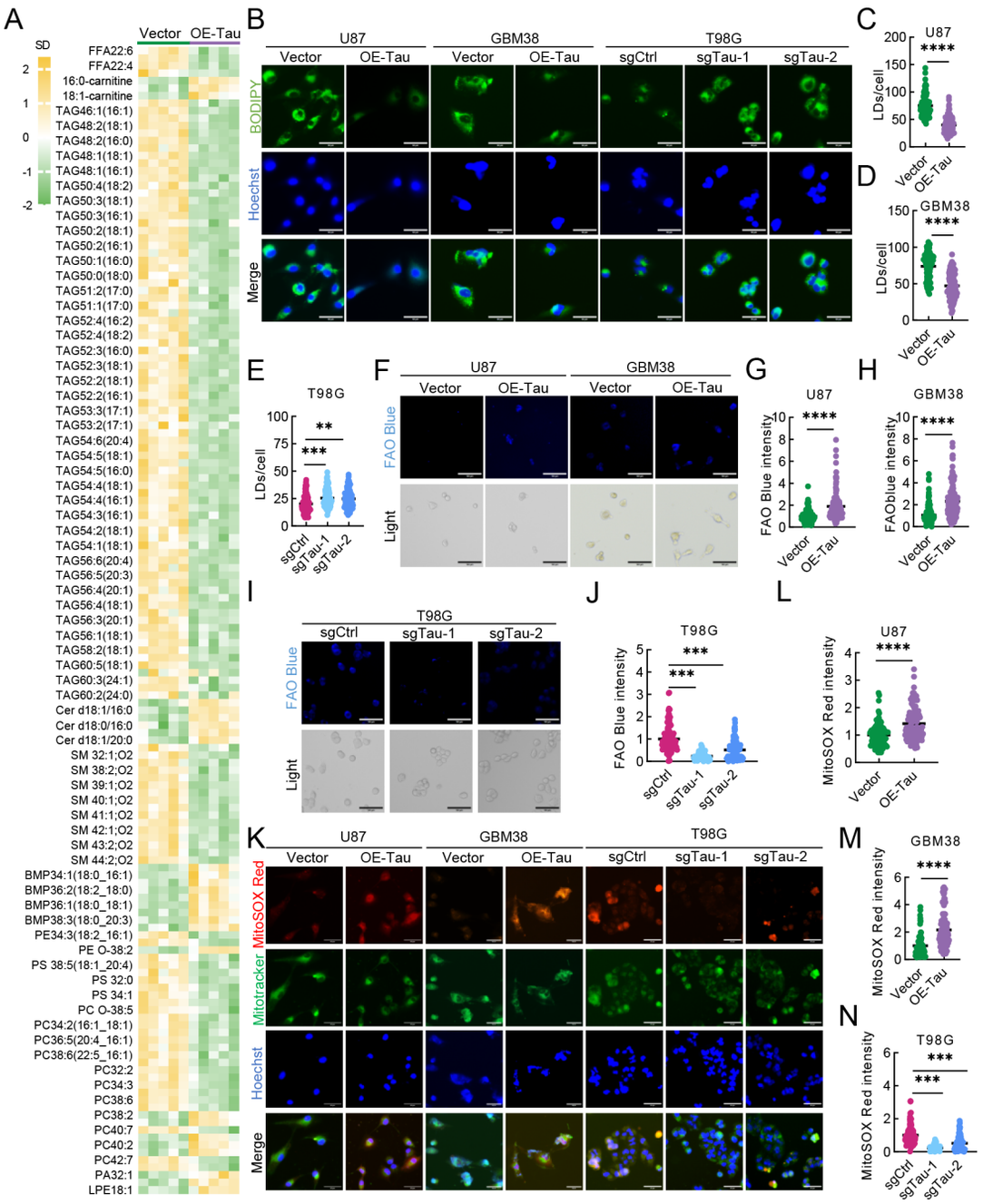

Figure 4 Tau enhances free fatty acid (FFA) β-oxidation

A: Heatmap showing relative abundance of significantly altered lipid species in U87 cells infected with tau or vector control, as determined by lipidomic profiling. Data were analyzed by Mann-Whitney *U* test. TAG: Triglycerides; FFA: Free fatty acids; AC: Acylcarnitine; BMP: Bis(monoacylglycerol) phosphate; CER: Ceramide; SM: Sphingomyelin; Hexcer: Hexosylceramides. B: Representative fluorescence images of lipid droplets (LDs) stained with BODIPY 493/503 (green) and nuclei stained with Hoechst 33342 (blue) in U87, GBM38, and T98G cells infected as indicated. Scale bar: 50 μm. C–E: Quantification of LD number per cell in U87 (C), GBM38 (D), and T98G (E) cells. *n*=100 per group. F: Representative images of FAO Blue staining (blue) and corresponding bright-field images in U87 and GBM38 cells infected with tau or vector control. Scale bar: 50 μm. G, H: Quantification of FAO Blue intensities in 100 cells. I, J: FAO Blue staining (I) and quantification (J) in T98G cells infected with sgctrl or sgTau. Scale bar: 50 μm; *n*=100 cells per group. L: Representative fluorescence imaging of mitochondrial ROS (red) detected with MitoSOX Red and mitochondria (green) by Mito-tracker Green in U87, GBM38 and T98G cells infected as indicated. Scale bar: 50 μm. K–N: Mitochondrial ROS levels were quantified in 100 cells. Data are presented as mean±SEM, analyzed by unpaired *t*-test (for C, D, G, H, L, and M) and one-way ANOVA (for E, J, and N). **: *P*<0.01; ***: *P*<0.001; ****: *P*<0.0001.

poorly understood. This study demonstrated that tau impedes glioma progression by enhancing FAO, thereby inducing genotoxic stress and triggering cellular senescence.

Tau, a well-established pathological factor in Alzheimer's disease and other tauopathies, displays markedly lower expression in glioma compared to normal brain tissue. Unlike its pathological accumulation in neurodegenerative disorders, reduced levels in glioma are positively correlated with malignancy and adverse prognosis, indicating a context-specific role in tumor suppression. Previous studies have

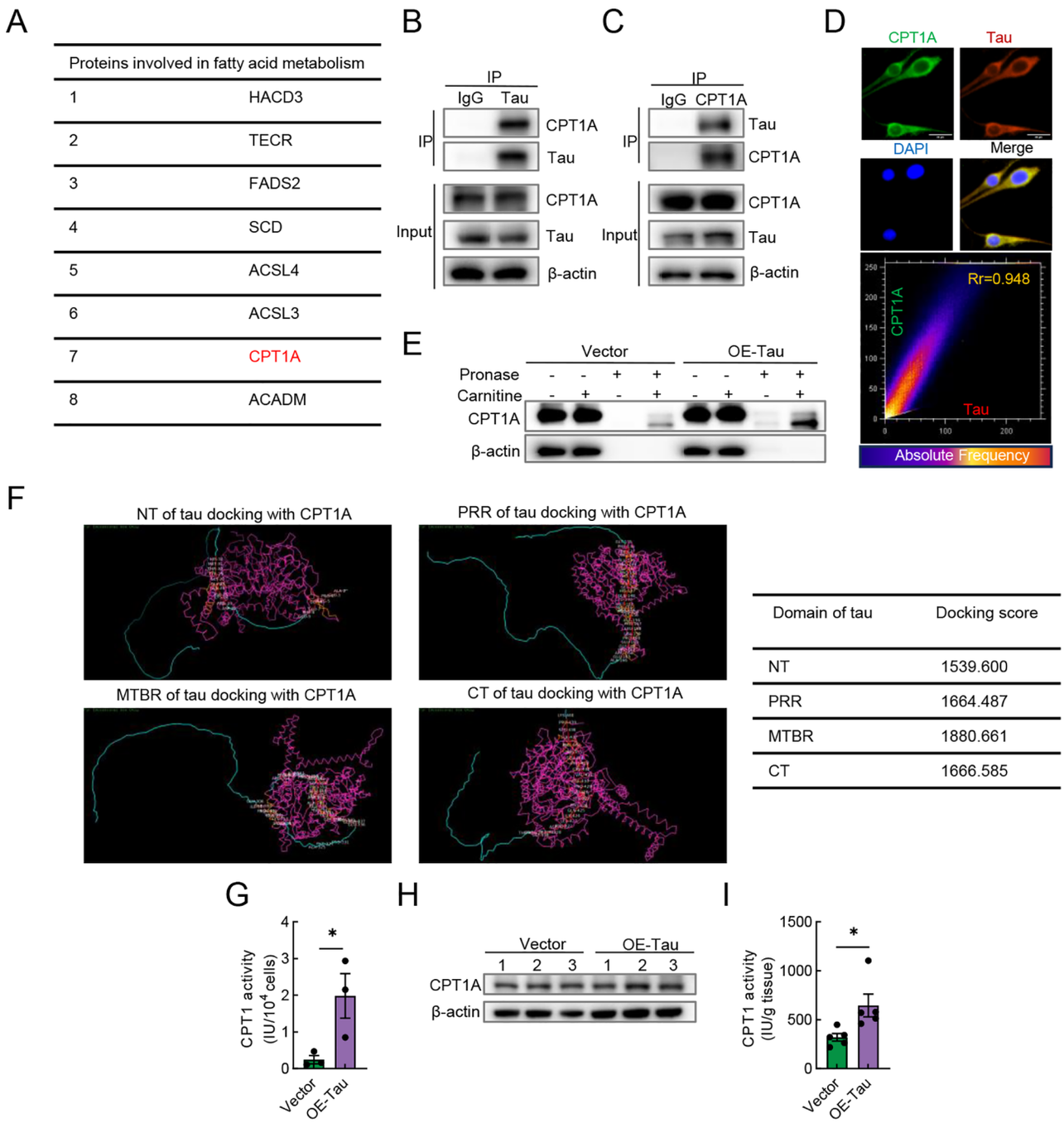

Proteins involved in fatty acid metabolism	
1	HACD3
2	TECR
3	FADS2
4	SCD
5	ACSL4
6	ACSL3
7	CPT1A
8	ACADM

Domain of tau	Docking score
NT	1539.600
PRR	1664.487
MTBR	1880.661
CT	1666.585

Figure 5 Tau interacts with CPT1A and enhances its enzymatic activity

A: List of proteins immunoprecipitated by tau and implicated in fatty acid metabolism. B, C: Interaction between tau and CPT1A, validated by immunoprecipitation with anti-IgG/tau and anti-IgG/CPT1A antibodies in U87 cell lysates. D: Representative immunofluorescence images showing co-localization of tau and CPT1A, quantified using ImageJ. E: Western blot analysis of CPT1A stability in U87 cells overexpressing tau, with or without carnitine treatment following DARTS assay. F: Docking model of truncated tau bound to CPT1A, showing interaction interfaces and docking scores. NT: N-terminal; PRR: Proline-rich region; MTBR: Microtubule binding region; CT: C-terminal; Turquoise: Tau; Pink: CPT1A; Red: Region in tau interacting with CPT1A; Brown: Region in CPT1A interacting with tau. G: CPT1 enzymatic activity in U87 cells transfected with tau or vector control. *n*=3 per group. H: Western blots of CPT1A in subcutaneous tumor xenografts. *n*=3 per group. I: CPT1 activity in subcutaneous tumor xenografts. *n*=5 per group. Data are presented as mean±SEM, analyzed by unpaired *t*-test. *: $P<0.05$.

suggested that tau regulates GBM progression by modulating the EGFR/NF-kB/TAZ mesenchymal axis (Gargini et al., 2020) or impairing cell migration (Nakata et al., 2020). Consistent with these observations, our results confirmed that elevated tau expression impedes glioma proliferation. Notably, mechanistic analyses discovered a pathway in which tau enhances FAO, thereby inducing DNA damage and cellular senescence.

Recent reports have identified divergent effects of tau overexpression on LD abundance, with a reduction observed in glial cells (Goodman et al., 2024) and an increase reported in neurons (Li et al., 2024). In glioma models, LD content was significantly reduced following tau overexpression, implicating tau as a regulator of LD homeostasis in this context. In

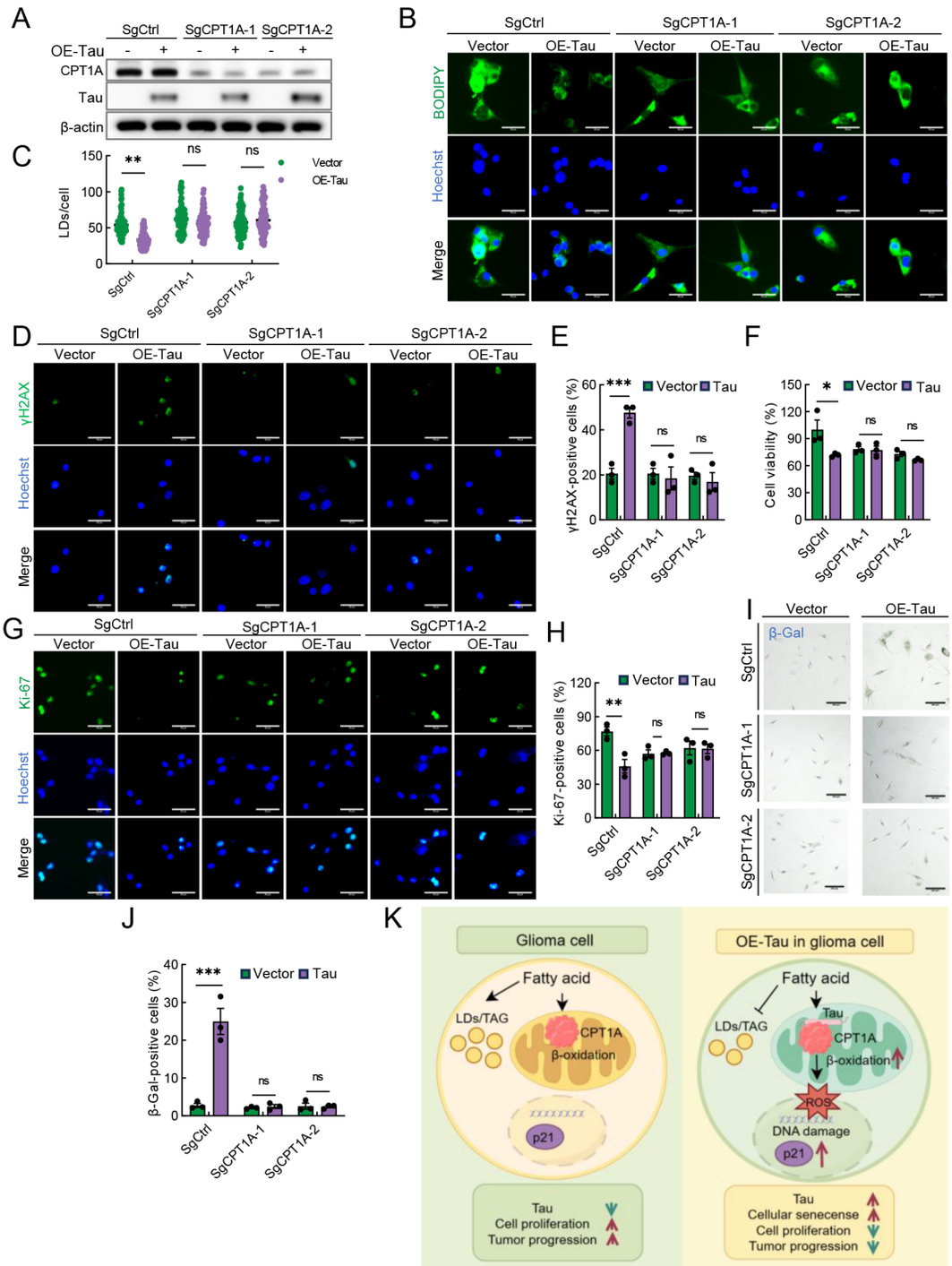

Figure 6 Tau promotes glioma cellular senescence in a CPT1A-dependent manner

A: Western blot analysis of tau and CPT1A expression in U87 cells infected as indicated. B: Representative fluorescence images of lipid droplets (LDs) stained with BODIPY 493/503 (green) and nuclei stained with Hoechst 33342 (blue) in U87 cells infected as indicated. Scale bar: 50 μm. C: Quantification of LD number in U87 cells infected as indicated (*n*=100). D, E: Representative γH2AX (green) immunofluorescence images (D) and quantification of γH2AX-positive nuclei (E) in U87 cells infected as indicated. Scale bar: 50 μm. *n*=3 per group. F: Cell viability of U87 cells infected as indicated. *n*=3 per group. G, H: Representative Ki-67 (green) immunofluorescence images (G) and quantification of Ki-67 positive cells (H). Scale bar: 50 μm. *n*=3 per group. I, J: Representative β-galactosidase staining images (I) and quantification of β-galactosidase-positive cells (J) in U87 cells infected as indicated. Scale bar: 200 μm. *n*=3 per group. K: Schematic model summarizing the role of tau in regulating lipid homeostasis and cellular senescence in glioma cells. Data are presented as mean±SEM, analyzed by two-way ANOVA. *: *P*<0.05; **: *P*<0.01; ***: *P*<0.001; ns: Not significant.

conjunction with previous findings, these observations suggest that tau exerts cell type-specific modulatory effects on lipid metabolism. The underlying basis for this differential response remains unresolved; however, several plausible mechanisms may explain the context-dependent actions of tau. One possibility stems from the distinct lipid metabolic profiles of neurons and glial cells. Neurons exhibit limited intrinsic capacity for fatty acid metabolism and rely on astrocyte-

mediated trafficking of FFAs for LD synthesis or β-oxidation via neuron-glia metabolic coupling (Ioannou et al., 2019; Mukherjee and Suresh, 2019). Another potential determinant is the differential expression of CPT1A, a key enzyme in mitochondrial fatty acid transport. Analysis of transcriptomic and proteomic data from the Human Protein Atlas revealed that CPT1A is selectively expressed in astrocytes, microglia, and vascular cell populations, but absent in neurons and oligodendrocytes. This distribution suggests that the capacity for FAO differs markedly across brain cell types. These findings support the hypothesis that the contrasting effects of tau on LD abundance may reflect variable CPT1A expression and divergent metabolic architecture between neuronal and glial lineages. Nonetheless, definitive validation will require targeted functional studies to elucidate the mechanistic relationship between tau, CPT1A, and lipid metabolism in a cell type–specific manner.

Tau is classically recognized for interacting with microtubules, whose instability is a significant causative factor in Alzheimer's disease (El Mammeri et al., 2022; Horie et al., 2021; Tan et al., 2019). Recent proteomic studies in human induced pluripotent stem cell (iPSC)-derived neurons have identified multiple mitochondrial proteins capable of binding tau, suggesting broader cellular roles beyond microtubule regulation (Tracy et al., 2022). Our research indicated that tau likely binds to CPT1A through the microtubule-binding region, resulting in enhanced enzymatic activity and up-regulated FAO in U87 glioma cells. However, whether this interaction interferes with microtubule association and whether such disruption contributes to the observed suppression of glioma cell proliferation in tau-overexpressing cells remains to be resolved.

CPT1A-mediated FAO has been described as a key energy resource that provides sufficient ATP for tumor cell growth (Duman et al., 2019). However, other studies have demonstrated that enhanced FAO can also induce cytotoxicity. For example, inhibition of DGAT1 has been shown to elevate CPT1A expression, increase FAO and ROS production, induce tumor cell apoptosis, and ultimately suppress glioma growth (Cheng et al., 2020). The present study similarly showed that tau-driven enhancement of CPT1A activity inhibited glioma growth. However, the reasons why targeting CPT1A yields different outcomes across tumor types remain unresolved. A plausible explanation is that tumors differ in basal CPT1A expression and reliance on FAO, resulting in distinct metabolic outcomes when CPT1A function is perturbed. Thus, thorough assessment of CPT1A expression, metabolic flexibility, and oxidative tolerance will be essential to guide its potential therapeutic application.

Recent work has revealed that FAO can drive cellular senescence by regulating histone acetylation and inducing the expression of the cyclin-dependent kinase inhibitor p16INK4a (Yamauchi et al., 2024). The present findings revealed that overactivation of FAO triggered by tau resulted in DNA damage and senescence in glioma cells, accompanied by increased expression of p21. However, the divergent effects of CPT1A activity and FAO on tumor behavior remain poorly defined. Further investigation is required to delineate the molecular and cellular factors that determine whether FAO promotes survival or induces cytotoxicity in tumor cells.

In summary, this study elucidated a regulatory axis in which tau engages CPT1A to promote FAO, leading to DNA damage and cellular senescence. These results provide mechanistic insight into the tumor-suppressive functions of tau in glioma, linking its expression to disease progression and patient outcomes. As such, tau may represent both a prognostic biomarker and a potential therapeutic target in glioma.

Considering the important regulatory role of tau in neurodegenerative diseases and nervous system function, the precise targeting of tau in glioma has become a necessary consideration in the development of innovative therapeutics. Strategies such as intracranial delivery of lipid nanoparticle-encapsulated plasmid DNA or mRNA encoding tau represent a potential avenue for therapeutic development. While this study has elucidated a role for tau in lipid metabolic regulation within glioma, whether this function exhibits subtype-specific heterogeneity or extends to other tumor types remains an open question that needs to be further explored.

DATA AVAILABILITY

All sequencing data were deposited in the Gene Expression Omnibus (GEO) Dataset (GSE294870), Genome Sequence Archive (GSA) database (https://ngdc.cncb.ac.cn/gsa-human) (GSA-Human: HRA011924), and Science Data Bank (doi: 10.57760/sciencedb.26421).

SUPPLEMENTARY DATA

Supplementary data to this article can be found online.

COMPETING INTERESTS

The authors declare that they have no competing interests.

AUTHORS' CONTRIBUTIONS

W.H.H., B.C.Z., and Z.X.W.: conceptualization; W.H.H., B.C.Z., W.J.Z., Z.W.L., and H.W.L.: investigation; W.H.H, W.J.Z., J.W.H., W.P.Z., X.S.Q., C.C., Y.Y.Z., Y.Y.X., and Y.Y.G.: methodology, software; W.H.H., B.C.Z., and Z.X.W.: writing–original draft preparation. All authors read and approved the final version of the manuscript.

REFERENCES

Bunker JM, Wilson L, Jordan MA, et al. 2004. Modulation of microtubule dynamics by tau in living cells: implications for development and neurodegeneration. *Molecular Biology of the Cell*, **15**(6): 2720–2728.

Casals N, Zammit V, Herrero L, et al. 2016. Carnitine palmitoyltransferase 1C: from cognition to cancer. *Progress in Lipid Research*, **61**: 134–148.

Ceccarelli M, Barthel FP, Malta TM, et al. 2016. Molecular profiling reveals biologically discrete subsets and pathways of progression in diffuse glioma. *Cell*, **164**(3): 550–563.

Cheng X, Geng F, Pan MX, et al. 2020. Targeting DGAT1 ameliorates glioblastoma by increasing fat catabolism and oxidative stress. *Cell Metabolism*, **32**(2): 229–242. e8.

Duman C, Yaqubi K, Hoffmann A, et al. 2019. Acyl-CoA-binding protein drives glioblastoma tumorigenesis by sustaining fatty acid oxidation. *Cell Metabolism*, **30**(2): 274–289. e5.

El Mammeri N, Dregni AJ, Duan P, et al. 2022. Microtubule-binding core of the tau protein. *Science Advances*, **8**(29): eabo4459.

Gargini R, Segura-Collar B, Herránz B, et al. 2020. The IDH-TAU-EGFR triad defines the neovascular landscape of diffuse gliomas. *Science Translational Medicine*, **12**(527): eaax1501.

Gargini R, Segura-Collar B, Sánchez-Gómez P. 2019. Novel functions of the neurodegenerative-related gene tau in cancer. *Frontiers in Aging Neuroscience*, **11**: 231.

Geng F, Cheng X, Wu XN, et al. 2016. Inhibition of SOAT1 suppresses glioblastoma growth via blocking SREBP-1-mediated lipogenesis. *Clinical Cancer Research*, **22**(21): 5337–5348.

Goodman LD, Ralhan I, Li X, et al. 2024. Tau is required for glial lipid droplet formation and resistance to neuronal oxidative stress. *Nature*

Neuroscience, **27**(10): 1918–1933.
Han WH, Zhang BC, Zhao WP, et al. 2025. Ketogenic β-hydroxybutyrate regulates β-hydroxybutyrylation of TCA cycle-associated enzymes and attenuates disease-associated pathologies in Alzheimer's mice. *Aging Cell*, **24**(1): e14368.
Hedna R, Kovacic H, Pagano A, et al. 2022. Tau protein as therapeutic target for cancer? Focus on glioblastoma. *Cancers*, **14**(21): 5386.
Horie K, Barthélemy NR, Sato C, et al. 2021. CSF tau microtubule binding region identifies tau tangle and clinical stages of Alzheimer's disease. *Brain*, **144**(2): 515–527.
Houten SM, Violante S, Ventura FV, et al. 2016. The biochemistry and physiology of mitochondrial fatty acid β-oxidation and its genetic disorders. *Annual Review of Physiology*, **78**: 23–44.
Ioannou MS, Jackson J, Sheu SH, et al. 2019. Neuron-astrocyte metabolic coupling protects against activity-induced fatty acid toxicity. *Cell*, **177**(6): 1522–1535. e4.
Khosla D. 2016. Concurrent therapy to enhance radiotherapeutic outcomes in glioblastoma. *Annals of Translational Medicine*, **4**(3): 54.
Lam SM, Zhang C, Wang ZH, et al. 2021. A multi-omics investigation of the composition and function of extracellular vesicles along the temporal trajectory of COVID-19. *Nature Metabolism*, **3**(7): 909–922.
Li YJ, Munoz-Mayorga D, Nie YH, et al. 2024. Microglial lipid droplet accumulation in tauopathy brain is regulated by neuronal AMPK. *Cell Metabolism*, **36**(6): 1351–1370. e8.
Miao H, Li BW, Wang ZH, et al. 2023. Erratum to "lipidome atlas of the developing heart uncovers dynamic membrane lipid attributes underlying cardiac structural and metabolic maturation". *Research*, **6**: 0185.
Miska J, Chandel NS. 2023. Targeting fatty acid metabolism in glioblastoma. *The Journal of Clinical Investigation*, **133**(1): e163448.
Mukherjee S, Suresh SN. 2019. Neuron-astrocyte liaison to maintain lipid metabolism of brain. *Trends in Endocrinology & Metabolism*, **30**(9): 573–575.
Nakata S, Price A, Eberhart C, et al. 2020. Increased tau expression correlates with IDH mutation in infiltrating gliomas and impairs cell migration. *Journal of Neuropathology & Experimental Neurology*, **79**(5): 493–499.
Shakya S, Gromovsky AD, Hale JS, et al. 2021. Altered lipid metabolism marks glioblastoma stem and non-stem cells in separate tumor niches. *Acta Neuropathologica Communications*, **9**(1): 101.
Tan R, Lam AJ, Tan T, et al. 2019. Microtubules gate tau condensation to spatially regulate microtubule functions. *Nature Cell Biology*, **21**(9): 1078–1085.
Tracy TE, Madero-Pérez J, Swaney DL, et al. 2022. Tau interactome maps synaptic and mitochondrial processes associated with neurodegeneration. *Cell*, **185**(4): 712–728. e14.
Velázquez AP, Tatsuta T, Ghillebert R, et al. 2016. Lipid droplet-mediated ER homeostasis regulates autophagy and cell survival during starvation. *Journal of Cell Biology*, **212**(6): 621–631.
Wang LB, Karpova A, Gritsenko MA, et al. 2021. Proteogenomic and metabolomic characterization of human glioblastoma. *Cancer Cell*, **39**(4): 509–528. e20.
Weller M, Wick W, Aldape K, et al. 2015. Glioma. *Nature Reviews Disease Primers*, **1**: 15017.
Xiang JY, Alafate W, Wu W, et al. 2022. NEK2 enhances malignancies of glioblastoma via NIK/NF-κB pathway. *Cell Death & Disease*, **13**(1): 58.
Yamauchi S, Sugiura Y, Yamaguchi J, et al. 2024. Mitochondrial fatty acid oxidation drives senescence. *Science Advances*, **10**(43): eado5887.
Zaman S, Chobrutskiy BI, Sikaria D, et al. 2019. MAPT (Tau) expression is a biomarker for an increased rate of survival for low-grade glioma. *Oncology Reports*, **41**(2): 1359–1366.